Essential Readings in Light Metals: Electrode Technology for Aluminum Production.
Edited by Alan Tomsett and John Johnson.

FINITE ELEMENT MODELLING OF THERMAL STRESS IN ANODES

Peter S. Cook
Comalco Research Centre
15 Edgars Road, Thomastown
Victoria 3074 Australia

ABSTRACT

Three-dimensional finite element models have been developed to determine stress arising in reduction cell anodes due to temperature gradients and interaction with metal components. The model results here focus on two important aspects of the stress distribution and their implications for anode cracking.

1. The development of thermal shock stress early in the anode life is investigated, including the roles of bath heat flux, freeze formation and anode thermal conductivity.

2. Detailed models of the anode stub region show a high stress in the carbon at the base of the stubholes during steady operation. The sensitivities of this stress concentration to yoke parameters and material properties are determined.

INTRODUCTION

Carbon anodes play a central role in the production of aluminium in Hall-Heroult reduction cells. Thermal, electrical and mechanical aspects of their performance all have a large impact on overall smelter profitability. Comalco has developed finite element models which solve the coupled temperature, voltage and stress distributions to enable optimisation of anode design. This paper focuses on mechanical aspects, providing an overview of the main factors controlling stress development from anode setting to withdrawal.

The carbon stress distribution has two important influences on anode performance. Firstly, excessive stress fractures the block with a consequent increase in anode voltage, power consumption, carbon consumption and process variability. Crack orientations are usually vertical, either longitudinal or transverse, or diagonal such that a lower anode corner is shed. Secondly, low stub-carbon resistance depends on closure of the airgap formed between cast iron and carbon after stub casting, and subsequent establishment of a contact pressure of at least 1 MPa[1].

Two previous studies of stress in reduction cell anodes have been published. Using a simplified anode and yoke geometry, Weng and Hsu[2] modelled the transient temperature distribution from anode setting until steady-state conditions were achieved. Associated changes in the carbon stress distribution and anode deformation were described. Kummer and Schmidt-Hatting[3] examined the stresses responsible for thermal shock spalling of anode corners, and their dependence on a number of anode variables.

The present paper provides a sensitivity analysis of carbon stress during both the initial 'thermal shock' stage and later steady operation. Earlier studies are extended by incorporating the effects of initial bath freezing and closure of the airgap between cast iron and carbon. The implications of the results for crack formation and propagation are discussed.

FINITE ELEMENT MODELS

A four-stub anode with block dimensions of 1650 mm by 910 mm by 550 mm was modelled (only one quarter by symmetry) using MSC/NASTRAN[4]. When modifying anode geometry for sensitivity analyses, care was taken to retain the same mesh in the regions of interest to avoid any mesh dependence. The yoke, stubs and cast iron were modelled as a single generic metal and material properties were approximated as temperature-independent. Values adopted for the baseline models are listed in Table I.

Table I: Baseline material properties for sensitivity study

Property	Carbon	Metal
Thermal conductivity, k (W/mK)	5.0	50
Specific heat, c (J/kg)	1200	500
Density, ρ (kg/m^3)	1600	8000
Thermal expansion coefficient, α (10^{-6}/K)	4.4	15
Young's Modulus, E (GPa)	4.8	200
Poisson's Ratio, ν	0.20	0.29

Anode carbon is weak in tension so Maximum Principal Stress, which defines the direction and magnitude of the greatest tensile component of stress at a given point, is often adopted as the simplest failure criterion. In this work, 'stress' and 'tensile stress' refer to Maximum Principal Stress unless otherwise stated.

Thermal Shock Model

When a new, cold anode is set in the molten cryolite bath, large temperature gradients result which create 'thermal shock' stresses within the carbon block. The finite element mesh (Figure 1) was concentrated around the anode base where stresses are highest.

Simple boundary conditions were applied to anode surfaces above the bath as their influence on thermal shock stress is minimal. Convective heat transfer from the anode top to an ambient temperature of 80°C was assumed, with an effective heat transfer coefficient of 2.5 W/m²K to include cover thermal resistance. Anode sides above the bath were treated as adiabatic.

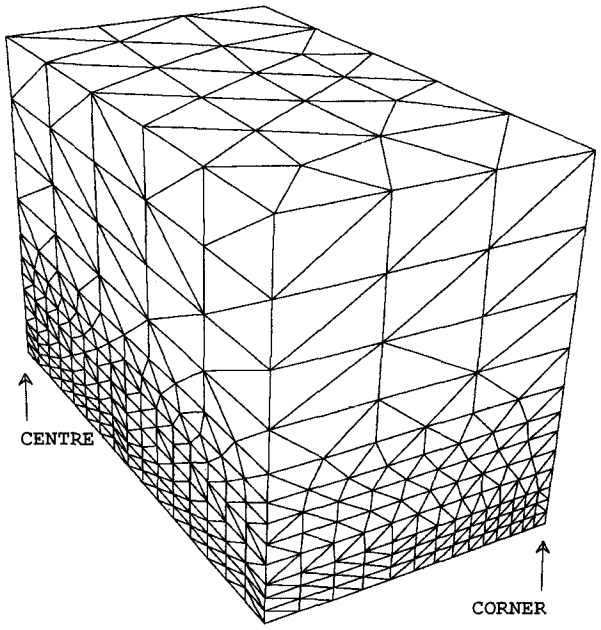

Figure 1. Finite element mesh for thermal shock model.

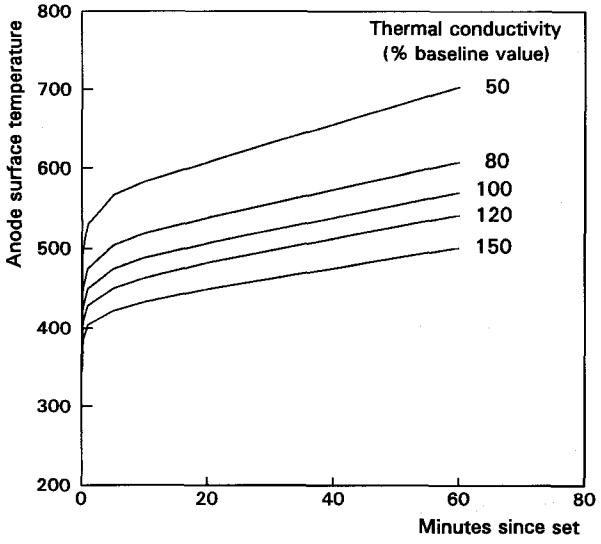

Figure 2. Immersed surface temperatures used in thermal shock model, for different carbon thermal conductivities.

A layer of bath freezes on the immersed surface of the cold anode (bottom 150 mm), and subsequently melts off. This behaviour was incorporated in the model by proscribing the time-dependence of the anode surface temperature where immersed (Figure 2). Surface temperature variation was extracted from a separate 1D transient model of bath solidification and remelting, validated by carbon temperature measurements, which incorporated bath latent heat. The heat flux from bath into the freeze was set at 20 kW/m² for the baseline case to produce complete remelting of freeze in four hours.

Steady-State Model

A stylised four-stub assembly (Figure 3) was employed to investigate the effects of the main design features on carbon stress. The stubhole had no taper or fluting and the yoke arm was a horizontal bar. A temperature distribution to approximate an anode operating in thermal equilibrium was applied; temperatures decreased linearly from 1000°C at the anode base to 800°C at the anode top, and then to 200°C at the assembly centre.

Contact between the metal and carbon was simulated with non-linear GAP elements. These have zero stiffness when open but exert a normal reaction force and friction when

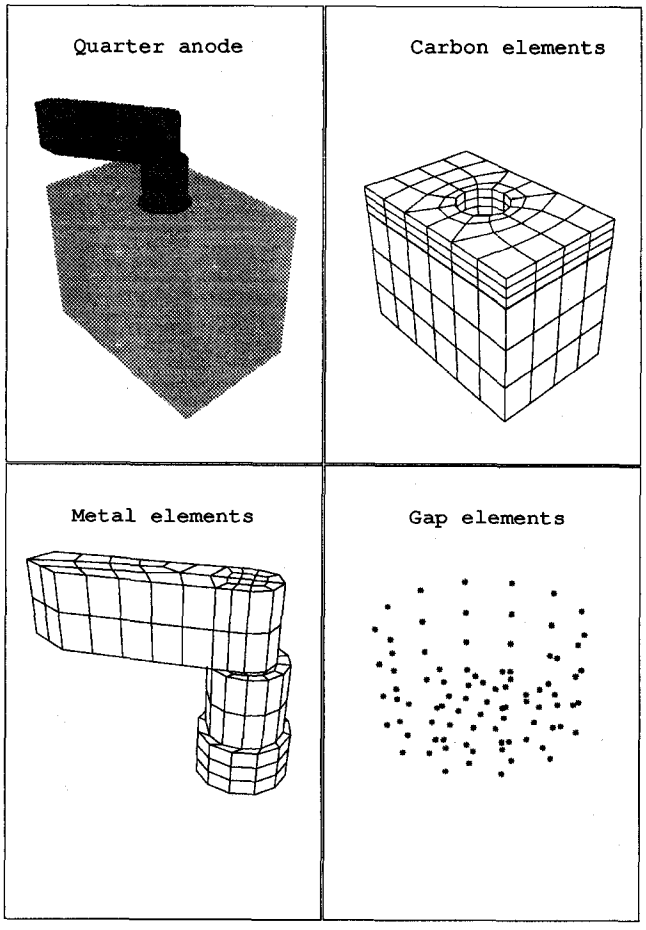

Figure 3. Finite element mesh for steady-state model.

closed[4]. The airgap was initiated to 0.5 mm in the cold anode to mimic shrinkage after casting and allowed to close by subsequent thermal expansion in the reduction cell. When varying stub or stubhole diameter, the initial airgap was scaled according to cast iron thickness.

THERMAL SHOCK STRESS RESULTS

Form of Thermal Shock Stresses

When an anode is first set, expansion of the hot surface layer creates tension in the cold carbon immediately inside. Conversely, the surface is in compression due to restraint by the interior carbon. As heat conducts into the anode, the layer in tension moves progressively further upward and inward, following the region where $\nabla^2 T$ is largest. Figure 4 illustrates the developing stress distribution on a vertical plane from anode centre to corner.

An initial stress concentration occurs near the anode corners, resulting from local superposition of the tensile layers formed parallel to each immersed surface[3]. The stress direction is approximately along the anode space diagonal so leads to corner shedding when thermal shock is severe.

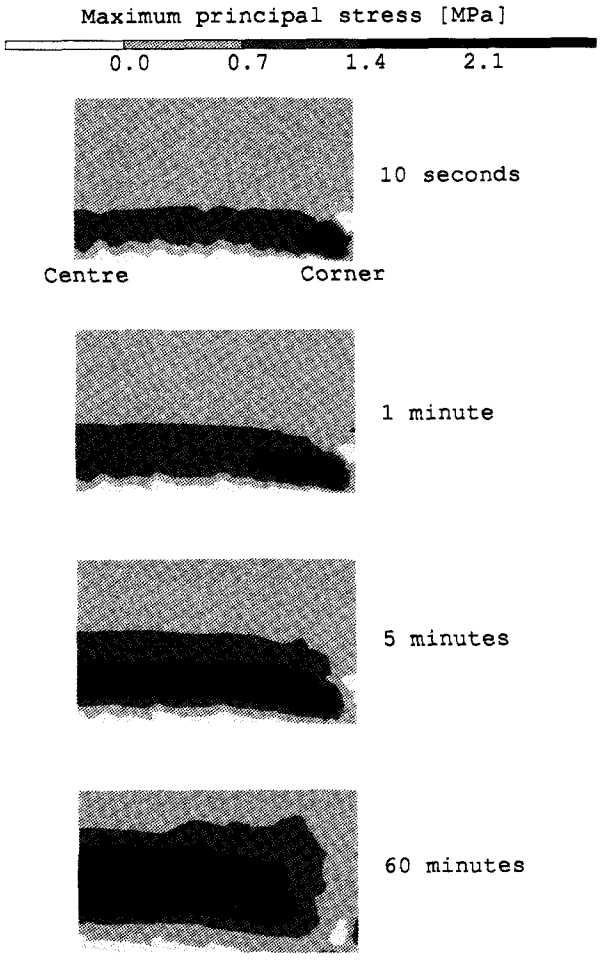

Figure 4. Stress distribution on vertical section through anode.

Stress within the tensile layer above the rest of the anode base ('Central stress') is relatively uniform. The thermal expansion load in the longitudinal direction (proportional to area of anode base and immersed sides) exceeds the transverse expansion load (base and immersed ends). Maximum Principal Stress is therefore directed along the anode length while Middle Principal Stress, still tensile but about 10% smaller for the modelled block dimensions, is transverse. This stress pattern explains the formation of vertical cracks by thermal shock and their usual bias toward transverse rather than longitudinal orientations.

Sensitivity Study

The variation of thermal shock stresses with key anode and process variables was investigated with a series of models modified from the baseline case. Central stresses were gauged by the peak stress attained 90 mm above the centre of the anode base and Corner stresses by the peak at the node 91 mm from the anode corner. (Stresses at other nodes show very similar sensitivities to changes in variables.) Table II summarises the results as a normalised stress sensitivity s_v for each variable v:

$$s_v = \frac{v_o}{\sigma_o}\left(\frac{\partial \sigma}{\partial v}\right)_o \qquad (1)$$

Here v_o is the baseline value of the variable and σ_o the corresponding peak Central or Corner stress. Note that stress is proportional to v^s for small departures from the baseline value v_o.

Table II: Response of peak stress to thermal shock variables

Variable	Normalised stress sensitivity (refer equation 1)	
	Central stress	Corner stress
Thermal conductivity	-0.3	-0.4
Young's Modulus	1.0	1.0
Thermal expansion coefficient	1.0	1.0
Anode length	-0.03	-0.003
Anode width	-0.3	-0.008
Anode height	-0.7	0.01
Immersion depth	0.2	0.1
Bath heat flux	0.05	0.02
Current draw dI/dt	<0.01	<0.01

Dependence on Carbon Thermal Conductivity

Both Central and Corner stresses decrease with conductivity (Figure 5), the basic reason being a lowered carbon temperature gradient. Higher conductivities increase the heat flux from the anode surface to interior, so the surface heats more slowly and the interior faster. However, the reduced surface heatup rate is partially offset by the resultant enhancement of heat flow through the frozen crust, this in turn being damped by an increase in crust thickness. Omission of these interactions with bath solidification leads to a sensitivity of stress to conductivity about double that obtained here[3].

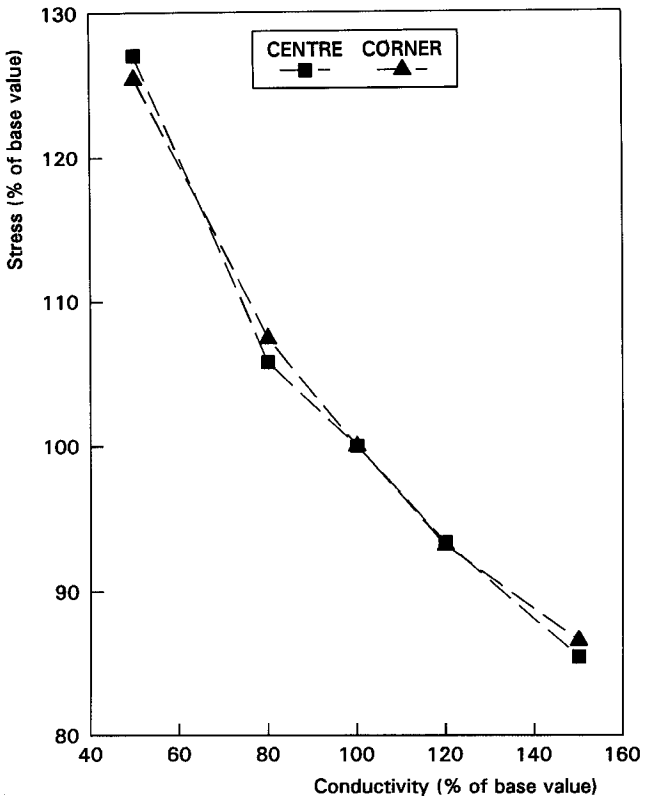

Figure 5. Sensitivity of Central and Corner stresses to carbon thermal conductivity.

Dependence on Immersion Depth

Thermal shock stresses increase with the initial depth of the anode in the bath (Figure 6), due to the greater expansion loading on the interior carbon. Corner stresses are generally more sensitive than Central stresses to immersion depth since anode sides contribute a large fraction of the corner loading. At larger depths, however, Corner stresses tend to saturate so display less sensitivity than Central stresses, as indicated in Table II for the baseline condition of 150 mm depth.

Dependence on Anode Dimensions

Corner stresses are virtually independent of anode dimensions (Table II) since they arise primarily from surface expansions in their immediate vicinity. Central stresses decrease strongly with increasing anode height (s = -0.7) since greater restraint by the top portion of the anode reduces the expansion and therefore tensile stress of the lower portion. Increasing the anode width also reduces Central stresses (s = -0.3) as the longitudinal expansion loading (proportional to area of base and immersed sides) increases more slowly with anode width than the volume of cold carbon to which it is applied. Anode length has negligible effect on Central stress (s = -0.03) since the expansion loading and stressed volume increase in the same proportion.

Dependence on Anode Current Draw

Resistive heating of the anode has negligible impact on thermal shock stresses. A simple calculation shows that resistive heating during the first hour is about two orders of magnitude smaller than conduction from the bath. Furthermore, the relatively even distribution of resistive heating through the block minimises any influence on the temperature gradients responsible for thermal shock.

Dependence on Other Carbon Properties

Thermal shock stresses are directly proportional to both the Young's Modulus and thermal expansion coefficient of the carbon. Stresses also increase with density and specific heat, and reduce with Poisson's Ratio, but there is little scope for variation of the latter three properties in plant production.

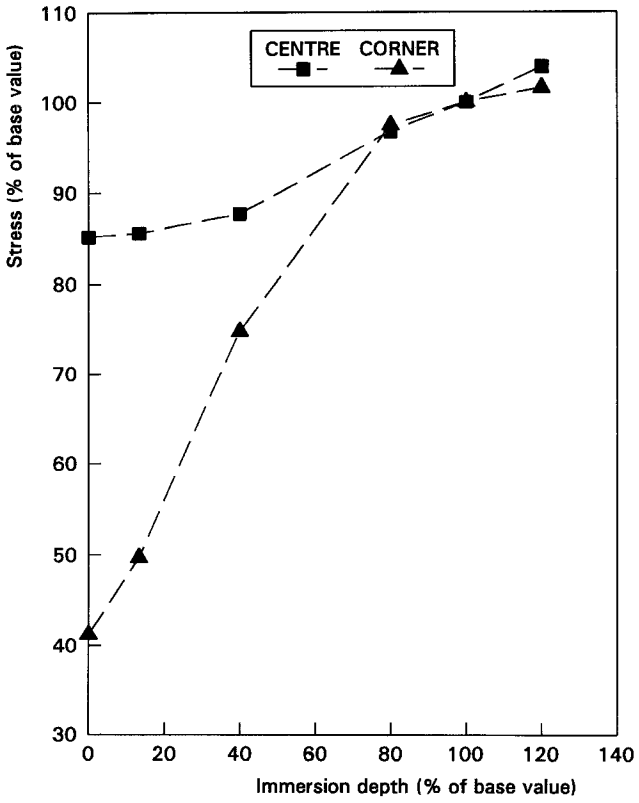

Figure 6. Sensitivity of Central and Corner stresses to depth of anode setting in bath.

STEADY-STATE STRESS RESULTS

Form of Steady-State Stresses

As the top of the anode reaches full operating temperature, radial thermal expansion of the stub and cast iron closes the initial airgap. High stresses around the stubhole result, greater on the outer side of the stubhole due to additional force from expansion of the yoke arms. The tendency of the carbon block to bow upward, due to the vertical temperature gradient, increases the influence of yoke arm expansion by pushing stubholes closer together. Peak tensile stresses occur at the outer edge of the stubhole base (Figure 7) which acts as a stress concentrator. A secondary stress maximum, of smaller magnitude but greater extent, occurs midway between the stubholes (Figure 7) as a result of yoke arm expansions.

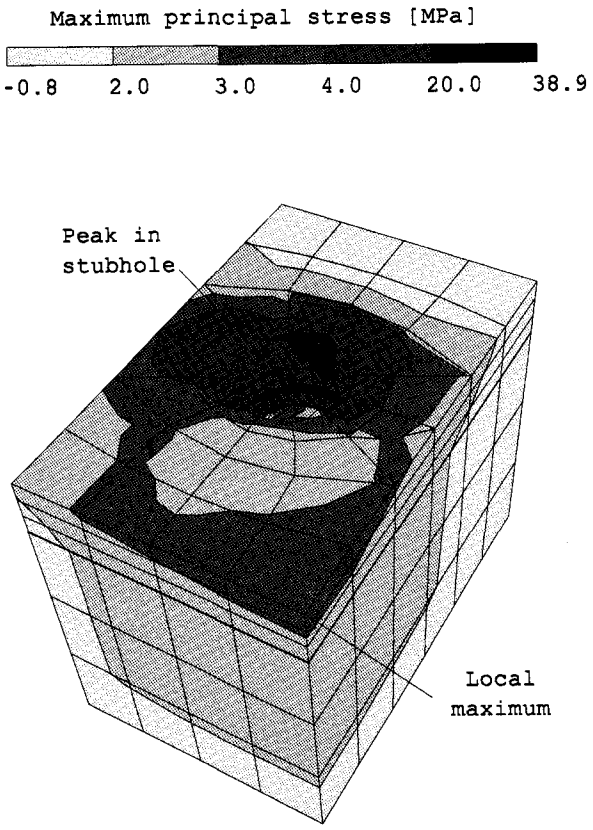

Figure 7. Steady-state carbon stress. [Note uneven contour scale]

Sensitivity Study

The response of the peak stubhole stress to a range of design and process variables was investigated. Results are expressed in terms of the normalised stress sensitivity defined by equation (1) and given in Table III. The sensitivities principally derive from the mismatch between stub/cast and stubhole expansions (mediated by the airgap) and changes in the flexibility of yoke arms and stubs.

Table III: Sensitivity analysis of peak stress during steady-state operation

Variable	Stress sensitivity (equation 1)
Temperature at base of rod	0.01
Temperature at top of block	1.1
Stubhole diameter	-0.3
Stubhole depth	-0.6
Stub diameter	0.4
Length of stub above block	-0.8
Length of yoke arm	0.7
Vertical thickness of yoke	1.2
Carbon Young's Modulus	0.3
Carbon thermal expansion coefficient	-0.4
Metal Young's Modulus	0.8
Metal thermal expansion coefficient	1.3

Dependence on Anode Height

Models were run at several reduced anode heights to examine the effect of anode consumption on stress levels. As the anode height decreases, it provides less restraint to expansion of the yoke arms. Carbon between the stubholes stretches further resulting in a considerable increase in the central stress concentration (Figure 8). Peak stubhole stresses, however, decline slightly due to the lower force applied by the yoke arms. The increase in anode top temperature and reduction in cross-sectional area with anode age (not modelled here) will tend to raise overall stress levels.

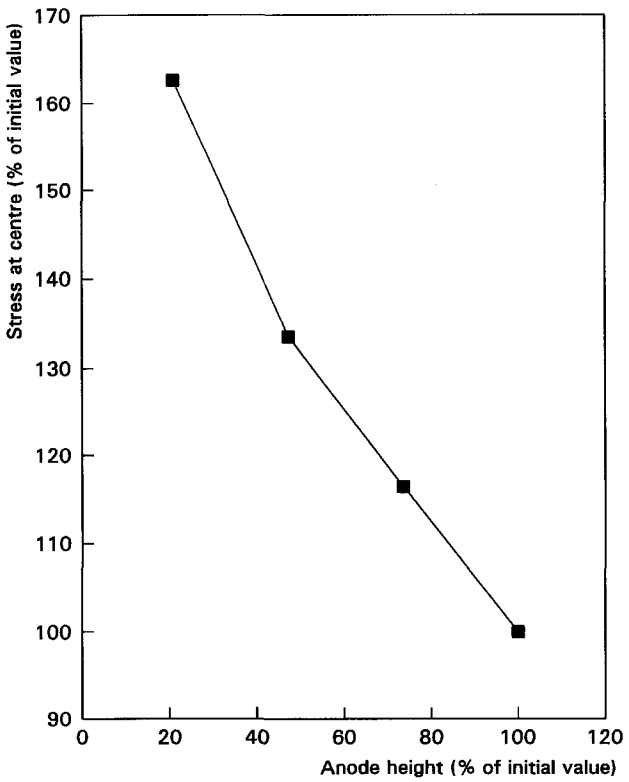

Figure 8. Increase in stress between stubholes with anode age.

IMPLICATIONS OF RESULTS FOR ANODE CRACKING

Sensitivity of Crack Probability to Anode Variables

Baked anode carbon behaves as a brittle material in which cracks usually initiate at pre-existing microscopic flaws. Thermal shock cracks have a corner-shedding or vertical orientation depending on the initiation point, in turn determined by the stress and flaw distributions. Anodes which survive thermal shock may still crack later from the assembly-dominated steady-state stresses.

Direct calculation of thermal shock fracture probability is difficult, requiring time integration over anode heatup of the fracture probability distribution. However, by approximating that the maximum stress reached is uniform in some volume and zero elsewhere, the effect on crack probability of small changes in anode variables (i.e. length, conductivity etc.) can

be estimated by Weibull statistics. The expressions obtained are functions of the existing crack rate, Weibull modulus 'm' and stress sensitivities. Details of the derivation are available on request.

A quantity termed Thermal Shock Fracture Resistance (TSFR) can be extracted for application to anode optimisation. This predicts relative trends in crack rate, rather than absolute changes, for small modifications to key variables. TSFR's to corner and vertical cracks differ due to unequal stress sensitivities (Table II):

$$TSFR_{VERTICAL} = \frac{k^{0.3}\ \sigma_c\ H^{0.7-0.5/m}\ W^{0.3-1/m}}{E\ \alpha\ B^{0.2}\ L^{1/m}} \quad (2a)$$

$$TSFR_{CORNER} = \frac{k^{0.4}\ \sigma_c}{E\ \alpha\ B^{0.1}} \quad (2b)$$

Both crack types increase with Young's Modulus E, thermal expansion coefficient α and (to a slight extent) bath immersion depth B. Both crack types decrease with the carbon Weibull characteristic strength σ_c (proportional to breaking strength) and (to a lesser extent) thermal conductivity k. Vertical cracks in good quality anodes ($m >> 1$) are also reduced by increasing anode height and slightly by increasing anode width.

The usual expression for thermal shock fracture resistance of ceramics[5] is $k\ \sigma_c / (E\ \alpha)$. Equations 2 extend this to include the effects of block dimensions, bath immersion depth and interaction with bath freeze formation. Kummer and Schmidt-Hatting[3] observed that anodes of high strength showed more tendency to thermal shock cracks, so moved σ_c to the denominator in their expression for fracture resistance. As they note, this implies that propagation rather than initiation of cracks may be the controlling factor.

Propagation of Cracks

Thermal shock cracks initiate with a large amount of stored strain energy. A rapid propagation of the crack beyond the critically-stressed region results[6], travelling a distance proportional to $\sigma_c\ (E\ \gamma)^{-0.5}$ where γ is the energy/unit crack area extension. Cracks initiating near a corner immediately propagate to the adjacent anode faces while vertical cracks extend across the anode base and typically 5 to 10 cm up the sides.

Propagation of vertical cracks then pauses until the stressed layer moves up with heat conduction to the level of the crack tip. Propagation may then recommence since, although the crack relieves overall stress levels slightly, the crack tip acts as a stress concentrator. Also, peak thermal shock stress increases with time (Figure 4).

Any subsequent propagation occurs stably over a period of hours, driven by the advancing heat front toward the top of the anode. Expansion of the assembly begins to influence the stress distribution after several hours. Stress levels below the stubholes build as stub expansion closes the airgap, causing a tendency for cracks to deviate preferentially toward stubholes. In steady-state, tensile stresses occur between and (especially) around the stubholes. Vertical cracks completely outside this region are therefore uncommon.

Resistance to Crack Propagation

The traditional approach to describing the resistance of materials to thermal shock damage is to relate stored strain energy to crack surface energy. A thermal shock propagation resistance is obtained:

$$TSPR = \frac{E\ \gamma}{\sigma_c^2} \quad (3)$$

A more recent method is to plot the critical stress intensity factor at the crack tip required for propagation as a function of crack length. The 'R-curve' obtained provides information about crack toughening behaviour. For carbon materials[7,8], the R-curve increases at small crack lengths due to the development of toughening mechanisms (crack bridging and microcracking) and then plateaus.

Anode fracture toughness can be increased by coarsening the microstructure to reduce crack severity by limiting unstable propagation (energy approach of equation 3) and/or enhancing resistance to stable propagation (R-curve approach). However, these gains must be balanced against a possible increase in crack frequency since crack initiation and propagation have opposite dependencies on Young's Modulus and strength. (Compare equations 2 and 3).

Discussion

Correlations of bulk anode properties with thermal shock tendency have been published by several authors. The dependence of thermal shock-related properties (strength, Young's Modulus, expansion coefficient, conductivity) on conditions of anode manufacture (raw materials, mixing, forming, baking) has been investigated using plant[9] and laboratory[10-13] anodes. The propensity of anode carbon to thermal shock cracking, as measured by a laboratory test involving rapid heating of a carbon disc, has also been examined[10-13]. The percentage of plant anodes cracked has been qualitatively compared with bulk properties[14] and laboratory thermal shock test results[13].

However, three important areas remain largely unexplored. The roles of initiation, unstable propagation and subsequent stable propagation as controlling factors in anode cracking need to be established. Secondly, there is a need for quantitative correlation of laboratory based thermal shock measures with the type, frequency and severity of anode cracks during operation. Finally, an expression for the cost to a smelter of anode cracking is necessary for proper evaluation of anode optimisation work. This should incorporate at least the relative frequencies and costs of corner shedding, vertical thermal shock cracks and steady-state cracks.

Although there is no definitive prescription as yet for eliminating thermal shock damage, some general guidelines arise from this and earlier work. The preliminary but essential steps are to remove special causes of low strength (e.g. gross pre-existing cracks) and then minimise common causes of inter-anode variability. For example, VALCO greatly alleviated a corner shedding problem by better control of the coke fines fraction[15]. Intra-anode variability (on a sub-cm scale) appears desirable for promoting fracture toughness. Further work is required in this area to balance the conflicting mechanical property requirements for

resistance to crack initiation and propagation, complicated by strong correlation between anode properties[3]. Crack initiation can be significantly reduced by altering carbon thermal conductivity or thermal expansion coefficient (refer equations 2) provided other properties remain unchanged. The rate of vertical thermal shock cracks can also be reduced slightly by setting the anode high and (if the carbon Weibull modulus is large) increasing anode height and width. Bath superheat or heat flux have negligible influence on thermal shock provided some freeze formation occurs.

CONCLUSIONS

1. Initiation and propagation of the two main types of thermal shock cracks have been explained in terms of the modelled transient and steady-state stress distributions.

2. Anode cracking probabilities are best interpreted by a statistical treatment based on the weakest-link concept.

3. On this basis, the response of crack rate to modification of key anode variables has been determined from stress model results (equations 2). Crack probability increases with Young's Modulus, thermal expansion coefficient and bath immersion depth, and decreases with strength and thermal conductivity. Anode dimensions have negligible effect on corner cracks, but do affect vertical cracks in a manner dependent on the carbon flaw strength variability. Bath heat flux is unimportant, except that cell conditions which prevent anode freeze formation will increase the crack rate considerably.

4. The dependence of cracks initiated by the assembly on material properties, geometry and anode age has been described.

References

1. D.G. Brooks and V.L. Bullough, "Factors in the Design of Reduction Cell Anodes", Light Metals, 1984, 961-976.

2. T. Weng and M.B. Hsu, "Temperature and Stresses in Carbon Anodes in an Aluminium Reduction Cell", Light Metals, 1984, 977-987.

3. E. Kummer and W. Schmidt-Hatting, "Thermal Shock in Anodes for the Electrolytic Production of Aluminium", Light Metals, 1990, 485-491.

4. MSC/NASTRAN Version 67, MacNeal-Schwendler Corporation, Los Angleles.

5. G.A. Schneider, "Thermal Shock Criteria for Ceramics", Ceramics International, 17 (1991) 325-333.

6. D.P.H. Hasselman, "Unified Theory of Thermal Shock Crack Initiation and Crack Propagation in Brittle Ceramics", J. Am. Ceram. Soc., 52 (1969) 600-604.

7. C. Schubert, H.A. Bahr and H.J. Weiss, "Crack Propagation and Thermal Shock Damage in Graphite Disks Heated by a Moving Electron Beam", Carbon, 24 (1986) 21-28.

8. B. Allard et al., "Fracture Behaviour of Carbon Materials", Carbon, 29 (1991) 457-468.

9. S.R. Brandtzaeg, O. Lid and J. Arntzen, "Anode Quality Related to Operational Parameters by Baking. A Comprehensive Large Scale Test", Light Metals, 1987, 597-602.

10. J.A. Brown and P.J. Rhedey, "Characterisation of Prebaked Anode Carbon by Mechanical and Thermal Properties", Light Metals, 1975, 253-269.

11. D. Belitskus, "Effects of Coke and Formulation Variables on Fracture of Bench Scale Prebaked Anodes for Aluminium Smelting", Met. Trans. B., 9 (1978) 705-710.

12. D. Belitskus, "Effects of Butts Content, Green Scrap, and Used Potlining Additions on Bench Scale Prebaked Anode Properties", Light Metals, 1980, 431-442.

13. J. Bigot, "Study of Anode Manufacturing Parameters Influencing the Thermal Shock Resistance", Light Metals, 1990, 493-496.

14. W. Schmidt-Hatting, A.A. Kooijman and P. van den Bogerd, "Sensitivity of Anodes for Electrolytic Aluminium Production to Thermal Shocks", Light Metals, 1988, 253-257.

15. N.A. Ambenne and K.E. Ries, "Operating Parameters Affecting Thermal Shock Cracking of Anodes in the VALCO Smelter", Light Metals, 1991, 699-704.

Essential Readings in Light Metals: Electrode Technology for Aluminum Production.
Edited by Alan Tomsett and John Johnson.

Recommended Reading

Adams, A.N., J.P. Mathews, and H.H. Schobert. The use of image analysis for the optimization of pre-baked anode formulation (2002, pp. 547–552).

Adams, A.N., and H.H. Schobert. Characterization of the surface properties of anode raw materials (2004, pp. 495–498).

Al Hosni, S., et al. Sohar Aluminium's anode baking furnace operation (2011, pp. 859–863).

Allaire, C. Effect of the type of brick and mortar on the resistance to deflection of the flue walls in horizontal flue carbon baking furnaces (1994, pp. 551–564).

Allred, V.D. Rotary hearth calcining of petroleum coke (1971, pp. 313–329).

Alscher, A., et al. Ageing and rheological properties of binder pitches (1986, pp. 605–615).

Ambenne, N.A. Vertical anode cracking – the VALCO experience (1997, pp. 577–583).

Ameeri, J., K.M. Khaji, and W.K. Leisenberg. The impact of the firing and control system on the efficiency of the baking process (2003, pp. 589–594).

Augood, D.R., S.S. Jones, and H.J. Seim. Hydrocarbon emissions from pitch (1981, pp. 963–976).

Baillargeon, F., et al. Reduction of ahead of schedules anodes through anode rod quality control (1996, pp. 569–573).

Barrillon, E. Effects of anode texture on consumption (1974, pp. 1023–1038).

Barrillon, E. Influence of the quality of pitch on the characteristics of anodes for the electrolytic production of aluminum (1971, pp. 351–364).

Barrillion, E., and J. Pinoir. Use of high-sulphur cokes in the production of prebaked anodes (1977, pp. 289–299).

Bart, E.F., et al. Source factors in quinoline insoluble content of coal tar pitch (1981, pp. 479–495).

Beier, S., et al. FEM analysis of the anode connection in aluminium reduction cells (2011, pp. 979–984).

Beilstein, M., and M. Spangehl. Vibrocompacting machines for the moulding of green anodes-process development from the equipment supplier's point of view (1998, pp. 745–752).

Belitskus, D. Effects of formulation and heating rate on changes occuring during baking of bench-scale Hall cell anodes (1983, pp. 741–747).

Belitskus, D. Evaluation of volumetric anode mix formulation (1984, pp. 923–932).

Belitskus, D., and W.W. Hill. Properties of bench scale anodes produced using binder pitches varying in primary and secondary QI contents (1990, pp. 577–581).

Belitskus, D.L. An evaluation of relative effects of coke, formulation, and baking factors on aluminium reduction cell anode performance (1993, pp. 677–681).

Belitskus, D.L. Effects of petroleum coke calcination temperature and anode baking temperature on anode properties (1991, pp. 557–563).

Bigot, J. Study of anode manufacturing parameters influencing the thermal shock resistance (1990, pp. 493–496).

Bigot, J., M. Gendre, and J. Rotger. Fuel consumption: A key parameter in anode baking furnace (2007, pp. 965–968).

Boenigk, W., A. Niehoff, and R. Wildforster. Influence of QI content on binder pitch performance (1991, pp. 615–619).

Boero, J.F.R. A mathematical model of anode burning and factors affecting it (1983, pp. 867–884).

Bopp, A.F., G.B. Groff, and B.H. Howard. Influence of maximum temperature and heat-soak times on the properties of calcined coke (1984, pp. 869–882).

Bullough, V.L., H.C. Marshall, and C.J. McMinn. Some effects of sulfur in petroleum coke on the performance of anode in prebake alumina reduction cells (1971, pp. 411–423).

Bullough, V.L., H.C. Marshall, and J.W. Pendley. Some effects of coke calcination temperature on reduction cell voltage (1974, pp. 1007–1022).

Cahill, R.A., R.E. Gehlbach, and G.S. Tittle. Factors influencing the carboxy reactivity of calcined coke (2000, pp. 563–568).

Carroll, J., and A.P. Grobbelaar. Refractories for anode baking furnaces (1981, pp. 543–567).

Chmelar, J., et al. Coke quality effect on the grinding in the air swept ball mill circuit (2005, pp. 647–652).

Chmelar, J., and H. Linga. Use of eddy current separator in butts processing (2010, pp. 959–962).

Chollier-Brym, M.J., et al. Anode reactivity: Effect of coke calcination level (2009, pp. 905–908).

Claver, J.F., and B. Coste. Paste plant design and control - a new approach (1993, pp. 641–645).

Dernedde, E., et al. Kinetic phenomena of the volatiles in ring furnaces (1986, pp. 589–592).

Dernedde, E., et al. The leakage of air in horizontal flue ring furnaces (1987, pp. 591–595).

Dojc, D., W. Leisenberg, and D. Maiwald. Triple low–triple high, concepts for the anode plant of the future (2008, pp. 833–838).

Dreyer, C., N. Backhouse, and A. Pinoncely. Featuring the new AP-FCBA paste plant technology (2002, pp. 577–582).

Dumortier, P.M., et al. The dry scrubbing of anode bake oven fumes - problems and solutions (1986, pp. 939–946).

Edwards, L., F. Vogt, and J. Wilson. Coke blending at Anglesey Aluminum (2001, pp. 689–694).

Ellis, P.J., and J.D. Bacha. Shot coke (1996, pp. 477–484).

Ellis, P.J., and E.E. Hardin. How petroleum delayed coke forms in a drum (1993, pp. 509–515).

Emad, F., et al. In-line inspection of carbon anodes for use in aluminum production (1996, pp. 581–586).

Engvoll, M.A., H.A. Øye, and M. Sørlie. Gas reactivity inside industrial anodes (2002, pp. 561–568).

Engvoll, M.A., H.A. Øye, and M. Sørlie. Influence of bath contaminations on anode reactivity (2001, pp. 661–667).

Fassbender, K., A. Aryus, and J. Klein. Measures for improving the environmental conditions in a carbon plant (1977, pp. 393-435)

Fischer, W.K., F. Keller, and R.C. Perruchoud. Interdependence between anode net consumption and pot design, pot operating parameters and anode properties (1991, pp. 681–686).

Fischer, W.K., and R. Perruchoud. Factors influencing the carboxy- and air-reactivity behaviour of prebaked anodes in Hall-Heroult cells (1986, pp. 575–580).

Fischer, W.K., and R. Perruchoud. Influence of coke calcining parameters on petroleum coke quality (1985, pp. 811–826).

Foosnaes, T., et al. Dilatometry of granular and composite carbon (1990, pp. 571–574).

Frosta, S., and T. Naterstad. Loss of weight systems in continuous carbon production - a competitor to traditional belt scales (1984, pp. 1715–1725).

Gagne, J., et al. Anode butts automated visual inspection system (2008, pp. 895–898).

Gagne, J., et al. Anode stubs inspection system (2007, pp. 1021–1024).

Garbarino, R.M., et al. Particle degradation during coke handling (1995, pp. 545–548).

Gilmore, G.P., and V.L. Bullough. A study on the effects of anode coke sulphur content on the operation of side pin Soderberg cells (1982, pp. 741–752).

Goodes, C.G., J.A. Eady, and J.C. Nixon. Production of anode grade carbon from coal (1987, pp. 459–464).

Grandfield, J.F., and J.A. Taylor. The downstream consequences of rising Ni and V concentrations in smelter grade metal and potential control strategies (2009, pp. 1007–1011).

Grunspan, J. Slot cutting in anodes (2007, pp. 283–285).

Hagen, M., W. Hilgert, and R. Skiba. Results of operating a new RTO based fume treatment system at a baking furnace (2007, pp. 977–980).

Harry, P., and A. Tomsett. Electrode plant-larger anode assembly project (2007, pp. 1015–1020).

Holden, I., et al. New process control system applied on a closed baking furnace (2006, pp. 603–608).

Hollingshead, E.A., and P.J. Rhedey. An appraisal of pure electrode coke by solvent refining of coal as an alternative to petroleum coke (1979, pp. 589–606).

Hughes, C.P. Methods for determining the degree of baking in anodes (1996, pp. 521–527).

Hume, S.M., et al. A model for petroleum coke reactivity (1993, pp. 525–531).

Hyvernat, P., P. Fayet, and J.L. Lemarchand. Recent improvements to the anode production process - industrial applications and results obtained (1983, pp. 821–842).

Kandev, N., and H. Fortin. Electrical losses in the stub-anode connection: Computer modeling and laboratory characterization (2009, pp. 1061–1066).

Keller, F., and W.K. Fischer. Development of anode quality criteria by statistical evaluation of operational results in the electrolysis (1982, pp. 729–740).

Keller, F., and S. Oderbolz. Process controlled operation of baking furnaces (1985, pp. 1107–1123).

Jones, S.S., and E.F. Bart. The role of primary quinoline insolubles in pitch-coke bond formation in anode carbon (1991, pp. 609–613).

Jones, S.S., and R.D. Hidebrandt. Green coke volatile emission spectra (1981, pp. 423–440).

Larsen, B., and M. Sørlie. Settling and semi-coke formation during liquid pitch storage (1987, pp. 533–539).

Lazarou, R., et al. Carbon baking furnace fluewall brick quality trial (1995, pp. 627–631).

Liu, T., et al. Thermal shock crack initiation and propegation behaviour of carbon anodes (1995, pp. 733–740).

Maiwald, D., M. Schneider, and C. Krupp. Advanced cooling of anodes in an open ring type baking furnace (2002, pp. 615–619).

Mannweiler, U., W. Fischer, and R. Perruchoud. Carbon products: A major concern to aluminum smelters (2009, pp. 909–911).

Martirena, H. Laboratory studies on mixing, forming and calcining carbon bodies (1983, pp. 749–764).

Martirena, H., and J. Marletto. Thermal phenomena in anode baking furnaces (1980, pp. 531–543).

McHenry, E.R. Coal-tar/petro industrial pitches (1997, pp. 543–548).

Meier, M.W., R.C. Perruchoud, and W.K. Fischer. Production and performance of slotted anodes (2007, pp. 277–282).

Miotto, P., et al. A new method to start up fires in baking furnaces (2005, pp. 683–688).

Müftüoğlu, T., and R. Fernandez. The effects of feedstock and coke calcination degree on the properties of bench-scale anodes (1990, pp. 511–519).

Müftüoğlu, T., J. Thonstad, and H.A. Øye. A laboratory study of the anode carbon consumption during aluminium electrolysis (1986, pp. 557–562).

Narvekar, R., A.K. Mathur, and J. Botelho. Design criteria for petcoke calciners (2008, pp. 865–870).

Nelson, H.W. Viscosity stability of binders for Søderberg anodes (1963, pp. 321–329).

Neyrey, K., et al. A tool for predicting anode performance of non-traditional calcined cokes (2005, pp. 607–612).

Nguyen, Q.C. Properties of laboratory green coke anodes (1985, pp. 903–913).

Nofal, A., et al. Voltage drop at the stub-anode connection as related to the carbon equivalent of the cast iron collar (2010, pp. 1079–1084).

Ordronneau, F., et al. Meeting the challenge of increasing anode baking furnace productivity (2011, pp. 865–874).

Øye, B., et al. Optimization of the anode-stub contact: Material properties of cast iron (2010, pp. 1073–1078).

Peacey, J.G., J. Auton, and J. Kaiser. Reduced fuel consumption in Noranda Aluminium's open-pit anode baking furnaces (1983, pp. 777–789).

Perrucoud, R.C., and W.K. Fischer. Determination of the sodium sensitivity of petroleum coke (1991, pp. 581–584).

Perruchoud, R.C., M.W. Meier, and W.K. Fischer. Survey on worldwide prebaked anode quality (2004, pp. 573–578).

Peterson, R.W., and E.J. Seger. Pitch control of prebaked anodes by slump measurement (1980, pp. 443–454).

Pippin, B.H. The production of petroleum coke for aluminum cell anodes (1971, pp. 297–310).

Proulx, A.L. Optimum binder content for prebaked anodes (1993, pp. 657–661).

Racunas, B.J. Anode baking furnace thermal balance (1980, pp. 525–530).

Rhedey, P.J. Behaviour of isotropic petroleum coke in bench-scale anodes (1987, pp. 491–496).

Rhedey, P.J. Carbon reactivity and aluminium reduction cell anodes (1982, pp. 713–725).

Ries, K. Enhancing coke bulk density through the use of alternative calcining technologies (2009, pp. 945–949).

Rorvik, S., and H. A. Øye. A method for characterisation of anode pore structure by image analysis (1996, pp. 561–568).

Sadler, B.A., and S.H. Algie. Macrostructural assessment of sub-surface carboxy attack in anodes (1989, pp. 531–540).

Scalliet, R. A test of anode reactivity with carbon dioxide (1963, pp. 373–384).

Schmidt-Hatting, W., A.A. Kooijman, and P. van den Bogerd. Sensitivity of anodes for electrolytic aluminium production to thermal shocks (1988, pp. 253–257).

Schneider, J.P., and B. Coste. Thermal shock of anodes: Influence of raw materials and manufacturing parameters (1993, pp. 611–619).

Schreiner, H., et al. Modelling of packing petroleum coke fractions (1996, pp. 507–514).

Severo, D., et al. Recent developments in anode baking furnaces design (2011, pp. 853–858).

Sinclair, K.A., and B.A. Sadler. Improving carbon plant operations through the better use of data (2006, pp. 577–582).

Sinclair, K.A., and B.A. Sadler. Which strategy to use when sampling anodes for coring and analysis? Start with how the data will be used (2009, pp. 1037–1041).

Skogland, M. A survey of the Pah problem in the aluminium industry (1991, pp. 497–502).

Slagtern, A., et al. Thermal expansion of carbon materials calcined at various temperatures: Structure, pore volume and content of impurities (1987, pp. 449–457).

Smith, M.A., et al. An evaluation of the effect of dust granulometry on the properties of binder matrix bench scale electrodes (1991, pp. 651–655).

Solheim, A., et al. Energy recovery and amperage increase in aluminium cells by active cooling of the anode yokes (2009, pp. 1091–1096).

Sorlie, M., Z.L. Kuang, and J. Thonstad. Effect of sulphur on anode reactivity and electrolytic consumption (1994, pp. 659–665).

Stevenson, D.T. Anode baking furnace hydrodynamic flue modeling (1988, pp. 307–314).

Stokka, P. Green paste porosity as an indicator of mixing efficiency (1997, pp. 565–568).

Stokka, P. Mixing and baking of Soederberg paste (1985, pp. 925–933).

Tiba, P.R.T., et al. Systemic analysis of flue wall bricks used on anode baking furnaces (2010, pp. 1015–1019).

Tørklep, K. Viscometry in paste production (1988, pp. 237–244).

Turner, N.R. Improvements in anode binder pitches by advances in raw materials handling, manufacturing and transportation (1990, pp. 629–638).

Turner, N.R. Relative contributions from the binder and the aggregate to oxidation impurity levels in a model anode binder matrix (2001, pp. 701–707).

Turner, N.R. Tracking the carbonisation pathway of different pitches and pitch coke mixtures by crystallite height (Lc) and interlaying spacing (d002) measurement. Part 2 (1997, pp. 521–529).

Varin, P. Use of a mathematical model to determine ohmic drops in a prebake anode assembly (1981, pp. 313–324).

Vidvei, T., T. Eidet, and M. Sørlie. Paste granulometry and Soderberg anode properties (2003, pp. 569–574).

Vitchus, B., and F. Cannova. Understanding calcined coke bulk density-inventory (2007, pp. 1035–1038).

Vogt, F., et al. A preview of anode coke quality in 2007 (2004, pp. 489–493).

Vogt, M.F., G.R. Jones, and G.A. Tyler. The use of refractory lifters in coke calcination (1984, pp. 1697–1714).

Vogt, M.F., and R.D. Zabreznik. Coke properties and excess anode consumption (1989, pp. 443–447).

Weng, T.L., and M.B. Hsu. Temperature and stresses in carbon anodes in an aluminium reduction cell (1984, pp. 977–987).

Wombles, R.H., and J.T. Baron. Laboratory anode comparison of Chinese modified pitch and vacuum distilled pitch (2006, pp. 535–540).

Wombles, R.H., J.T. Baron, and S. McKinney. Evaluation of the necessary amount of quinoline insolubles in binder pitch (2009, pp. 913–916).